

Optimization of Cryogenic Detector Test Station by Rejecting Electromagnetic Interference

Sangbaek Lee^{a,1}, Whitney Armstrong^{a,*}, Maximo DiPreta^b, Jacob Dulya^{a,2}, Valentine Novosad^b, Tomas Polakovic^a

^a*Physics Division, Argonne National Laboratory, Lemont, IL 60439, U.S.A.*

^b*Materials Science Division, Argonne National Laboratory, Lemont, IL 60439, U.S.A.*

Abstract

We report on the solution optimized for characterizing SNSPDs by rejecting electromagnetic interference from various sources. The proposed readout method enhances measurement stability and enables reliable device characterization at low bias currents, where the signal-to-noise ratio is typically limited. By effectively suppressing EMI-induced noise, the method improves the ability to distinguish genuine detection events from spurious signals and reduces the effort required for data analysis. The approach has been applied to preliminary measurements of SNSPDs exposed to α particles emitted from a ^{241}Am source, demonstrating stable operation and clean signal acquisition. While a detailed study of α detection is underway, the method establishes a foundation for further characterization of SNSPDs with various incident particles. The demonstrated EMI rejection technique is expected to facilitate future research in particle detection and support ongoing SNSPD development for applications in nuclear and accelerator-based experiments.

Keywords: SNSPD, superconducting sensors, pair-breaking detectors

1. Introduction

Superconducting Nanowire Single-Photon Detectors (SNSPDs) are state-of-the-art devices designed to detect individual photons across a broad wavelength range, from the near-infrared to the X-ray region. Their operation relies on an abrupt change in resistivity that occurs when a photon is absorbed by the superconducting nanowire [1]. SNSPDs are distinguished by their exceptional timing resolution [2] and high detection efficiency [3], making them highly suitable for a wide range of advanced sensing and measurement applications [4].

While Superconducting Nanowire Single-Photon Detectors (SNSPDs) were originally developed to detect photons in the visible and near-infrared wavelength ranges, their capabilities extend well beyond these traditional applications. SNSPDs can also detect charged particles through two distinct mechanisms: one analogous to photon detection and the other governed by thermal processes [5]. The detection of charged particles has been demonstrated across a wide range of energies, including the keV [6, 7, 8, 9, 10, 11, 12], MeV [13], and GeV regimes [14]. The capability of SNSPDs to detect high-energy charged particles has drawn increasing interest for potential applications in future collider experiments, such as the Electron-Ion Collider (EIC) [14] and the Future Circular Collider (FCC) [15].

SNSPDs are typically characterized inside cryostat [16], where electromagnetic interference (EMI) from various sources

can contaminate the signal channels. While radio-frequency (RF) noise can often be mitigated using a Faraday cage or by the metallic enclosure of the cryostat itself, interference originating from three-phase motor components requires a careful analysis of the conductive paths [17]. In this paper, we present a simpler and more effective method to suppress such interference, enabling more precise detector characterization. This approach provides a practical foundation for building future SNSPD test systems. Characterization measurements have been performed at Argonne National Laboratory (ANL) using an alpha-particle source, which deposits significantly more energy in the nanowire than a 120 GeV proton [14]. The low-energy α particles emitted from the sealed source deposit substantial energy in the SNSPD, providing a valuable opportunity to investigate the ion detection mechanism and to optimize sensor designs for future collider experiments.

2. Experimental Setup

Figure 1 shows a schematic of the testbed inside the cryostat used to characterize α -particle detection with SNSPDs. Nanowire devices of different geometries were mounted inside a cryostat coupled to a Gifford-McMahon (GM) cryocooler. The fabrication of these devices has been described in previous studies [18, 14]. Each nanowire chip, with an active area of $10 \times 10 \mu\text{m}^2$, was wire-bonded to a PCB equipped with 50Ω shunt resistors. The assembly was mounted on a copper tee attached to the second stage of the GM cryocooler, maintaining a cryogenic temperature of $T = 2.7 \text{ K}$. The temperature at the PCB was monitored using a silicon diode sensor.

*Corresponding author

Email address: warmstrong@anl.gov (Whitney Armstrong)

¹Present Address: Temple University

²Present Address: Illinois Institute of Technology

The nanowire devices were tested both with and without a ^{241}Am source of $100\text{ }\mu\text{Ci}$ (equivalent to 3.7 MBq) mounted on a source holder. This source emits α particles with energies of 5.49 MeV (84.8%), 5.44 MeV (13.1%), and 5.34 MeV (1.7%), as well as significant hard X-rays at 59.54 keV (35.9%) and 26.34 keV (2.3%) [19]. Owing to the long penetration depth of these hard X-rays [20], a nanowire layer thickness on the order of 100 nm is typically required for X-ray sensitivity [21, 22]. The nanowire device used in this study was 12 nm thick, rendering it effectively insensitive to X-rays. To confirm this, an additional measurement was conducted with an α -shield, in which a 0.5 mm -thick stainless-steel layer was placed between the source and the sensor to block the α flux and isolate the response to X-rays. The distance between the radioactive source and the nanowire device was 4.85 mm , determined from the measured lengths of the standoffs and the source container.

Among possible superconducting nanowire material choices, Niobium has an advantage in its radiation hardness [23, 24, 25, 26] in the relatively higher operating temperature of Nb-compounds such as NbN. Performance of irradiated SNSPDs has been an interesting topic. It has been reported that there is no degradation of detection efficiency after irradiation over a few days [13]. Instead, improvement of detection efficiency at given bias current has been studied by controlling the switching current after defect by local alpha irradiation [27, 28, 29], but a fluence of this work is not relevant to those studies.

Fig. 2 presents the block diagrams for electronics setup. One of the nanowire channels (Wire1) was current-biased by an LTC1427 current output DAC (DC_1), with slow control managed by a Raspberry Pi 3 Model B. The signal from the wire was amplified by the Low Noise Amplifier (LNA_1) in the room-temperature electronics, followed by the fan-out. One of the fan-out outputs was recorded by an oscilloscope and another channel was delayed by 50 ns to form a trigger. Other part of trigger logic is to veto the EMI around the metal components including the cryostat and nanowire and primarily arising from the cold head motor and complex return paths surrounding them. This interference typically manifested as a short pulse on other wires when they were connected to other DAC (DC_INT), LNA (LNA_INT), and shared ground. The smallest width device on each chip (Wire_INT in Fig.2) was used as an antenna to generate negative pulse and as a veto. The DAQ livetime was estimated by counting veto events using a LeCroy 2551 Scaler in conjunction with a CAEN C111C Ethernet CAMAC Crate Controller. The effect of logic was studied by taking the reference data without using logic components, i.e., by taking the data with self-triggered LNA_1 output.

3. Results

Figure 3 shows the measured count rate as a function of bias current for three SNSPD devices with different geometries. In all panels, data are compared between measurements performed with and without EMI rejection, and with an additional α -shield when applicable.

(a) For the device with $w = 100\text{ nm}$ and $d = 10\text{ }\mu\text{m}$, the noise floor is significantly elevated when EMI rejection is not ap-

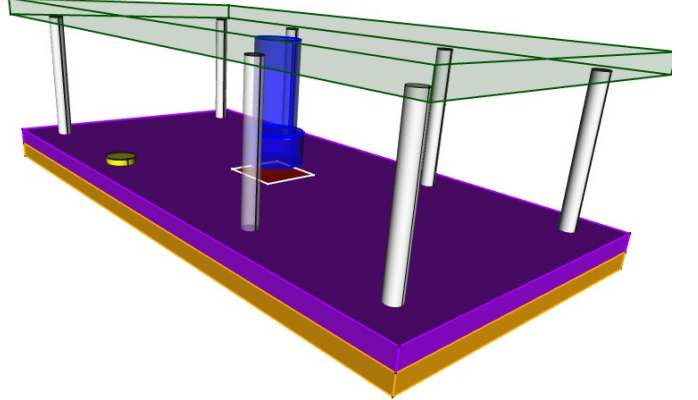


Figure 1: A schematic drawing of the testbed inside the cryostat (not-to-scale). The nanowire sensor (red) is wire-bonded to the PCB (purple). The PCB support (orange) is made of copper and attached to the second stage of the cryostat, temperature of which is monitored by the silicon diode sensor (yellow). The sealed source support (green) is fixated to the PCB support by standoffs.

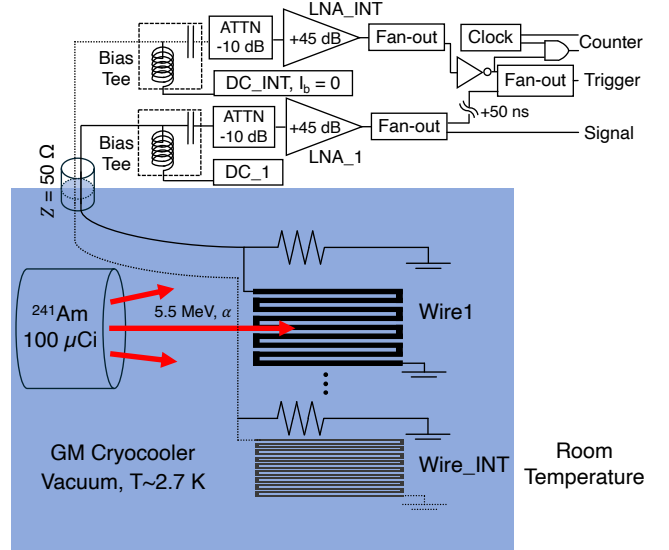


Figure 2: A block diagram depicts the electronic circuitry inside the cryostat (blue background) and outside (white background). The α particle detection was carried out by the nanowire device of interest (Wire1). The raw voltage waveform of signal and interference were monitored on the oscilloscope, with trigger logic implemented to veto interference signals.

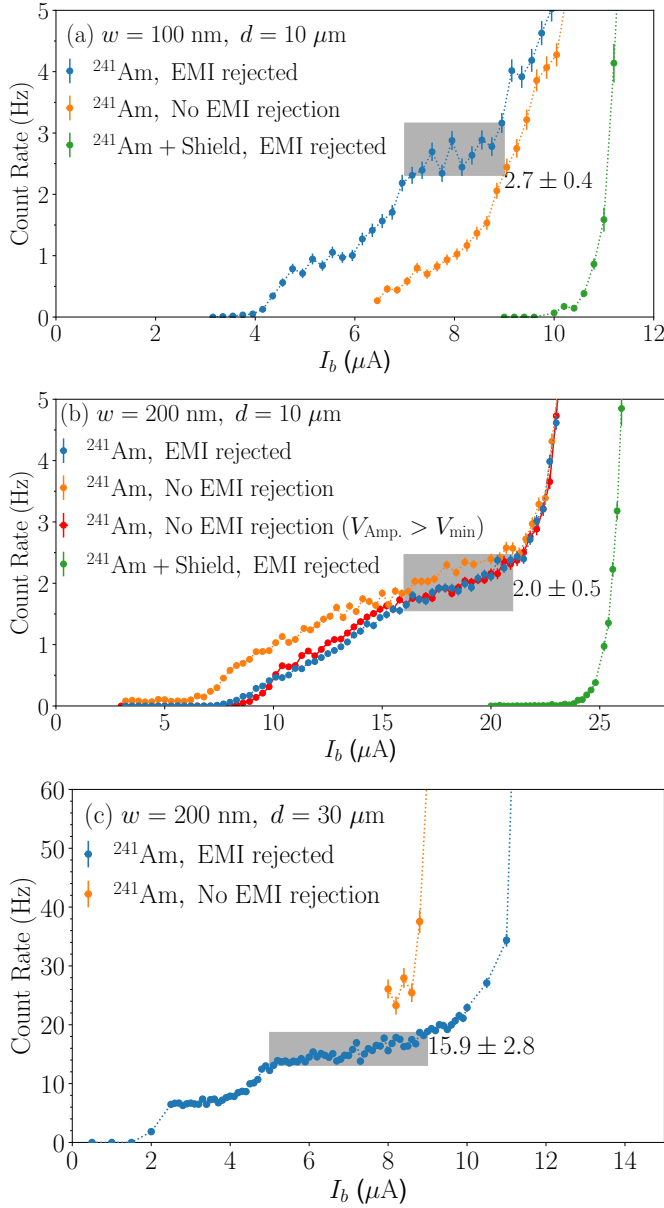


Figure 3: Measured count rates as a function of bias current for SNSPDs with varying geometries. Data are shown with EMI rejection (blue), without EMI rejection (orange), and with an additional α -shield (green) where applicable. The gray band and adjacent numbers indicate the estimated count rate at the plateau. (a) 100 nm-wide, 10 μm -long device: EMI suppression is essential at low bias to reveal α -induced counts above the noise floor. (b) 200 nm-wide, 10 μm -long device: EMI rejection removes spurious interference counts. For this case, rates measured with the minimum voltage amplitude condition defined in Fig. 4 (red) agree with the EMI-rejected data (blue). The minimum voltage is defined in Fig. 4. (c) 200 nm-wide, 30 μm -long device: EMI rejection is crucial for obtaining stable and reliable measurements of the SNSPD response.

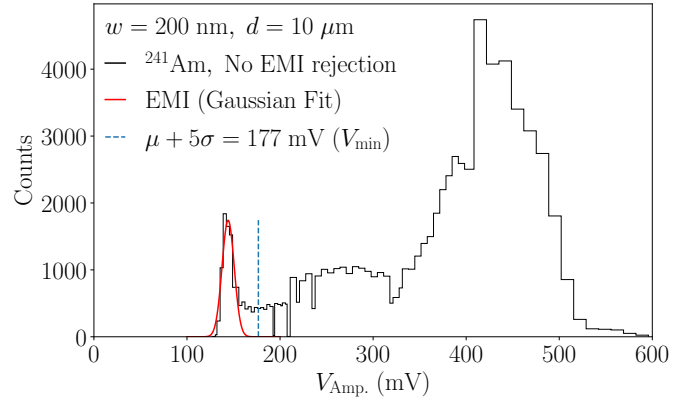


Figure 4: A histogram of V_{amp} for the dataset measured without EMI rejection using the device with $w = 200 \text{ nm}$ and $d = 10 \mu\text{m}$. The peak around 150 mV indicates substantial EMI contributions measured alongside genuine detector signals. This peak is fitted with a Gaussian profile, and $\mu + 5\sigma$ is adopted as the minimum voltage-amplitude threshold for Fig. 3, where μ and σ denote the mean and standard deviation of the Gaussian fit.

plied, requiring a higher detection threshold to obtain meaningful data. The measurements at lower bias currents are particularly valuable for characterizing the onset of α -induced counts; therefore, effective EMI suppression is crucial for achieving reliable results in this regime.

(b) For the device with $w = 200 \text{ nm}$ and $d = 10 \mu\text{m}$, the higher critical current enables measurements above the noise floor across the entire bias range. However, in the absence of EMI rejection, a substantial number of noise-induced events are observed, as evidenced by a nonzero count rate even at low bias currents (orange curve in Fig. 3). Implementing EMI rejection effectively suppresses these spurious counts (blue curve). Figure 4 shows the voltage amplitude (V_{amp}) histogram for the dataset measured without EMI rejection, where a Gaussian peak around 150 mV indicates the presence of such interference. This demonstrates that measurements without EMI rejection require a minimum voltage-amplitude threshold, defined here as 5σ above the mean of the Gaussian fit. Applying this threshold yields a count rate that agrees well with the EMI-rejected data, confirming that EMI rejection suppresses noise-induced events without affecting genuine detector responses. Moreover, the EMI rejection method does not require fitting V_{amp} or recording individual waveforms, enabling more efficient data acquisition.

For the devices used in measurements (a) and (b), similar measurements were also performed with a 0.5 mm-thick stainless steel shield. The application of the shield significantly reduces the observed counts, demonstrating that the detector response does not originate from γ rays emitted by ^{241}Am .

(c) For the larger-area device ($w = 200 \text{ nm}$, $d = 30 \mu\text{m}$), measurements without EMI rejection were not feasible due to the elevated noise level. With EMI rejection applied, the data exhibit a clean transition in count rate near the switching current, confirming stable detector operation and demonstrating the importance of interference suppression for large-area SNSPDs.

Given the long half-life of ^{241}Am (432.6 years) [19], the

α flux is considered stable. The count rate at the plateau is measured to be 2.6 ± 0.5 Hz for the 100 nm, 10 μm device; 2.0 ± 0.5 Hz for the 200 nm, 10 μm device; and 15.9 ± 2.8 Hz for the 200 nm, 30 μm device. These results are consistent with expectations that the energy deposited by α particles is sufficient for detection even in the narrower 100 nm wire. Furthermore, the count-rate ratio between the 30 μm and 10 μm devices is 7.95 ± 1.22 , in good agreement with the naive geometric estimation of a factor of 9.

4. Summary

We presented a readout method designed to reject EMI by using additional SNSPD on the same chip as an antenna, and thereby improve the signal fidelity in SNSPD measurements. This method enables reliable device characterization even at low bias currents, where the signal-to-noise ratio is typically limited. In addition, the approach allows researchers in SNSPD R&D to efficiently distinguish genuine signal waveforms from noise, saving both time and computational resources during data analysis.

While a detailed analysis of α -particle detection with SNSPDs is beyond the scope of this paper, our results demonstrate that SNSPDs can effectively register α events. The ability to detect α particles has important implications for a range of applications, including nuclear physics experiments, radiation monitoring, and particle identification studies.

Furthermore, the demonstrated EMI rejection and stable α detection performance highlight the versatility of SNSPDs as particle sensors beyond their traditional use as photon detectors. We anticipate that the methods and findings presented here will support future research in SNSPD-based particle detection and contribute to the development of high-precision, low-noise detection systems for both fundamental studies and applied technologies.

Acknowledgements

This material is based upon work supported by the U.S. Department of Energy, Office of Science, Office of Nuclear Physics, under contract number DE-AC02-06CH11357, the U.S. Department of Energy, the Office of Science under the Microelectronics Co-Design Research Project "Hybrid Cryogenic Detector Architectures for Sensing and Edge Computing enabled by new Fabrication Processes" (LAB 21-2491), and the U.S. Department of Energy, the Office of Science under the Co-design and Heterogeneous Integration in Microelectronics for Extreme Environments (CHIME) "Single Photon Detectors Integrated with Cryogenic Electronics (SPICE)" (LAB 24-3320). W. A. and T. P. acknowledge financial support from the U.S. Department of Energy, Office of Nuclear Physics, Early Career Award under grant number DE-FOA-0003176.

References

- [1] G. N. Gol'tsman, O. Okunev, G. Chulkova, A. Lipatov, A. Semenov, K. Smirnov, B. Voronov, A. Dzardanov, C. Williams, R. Sobolewski, Picosecond superconducting single-photon optical detector, *Applied Physics Letters* 79 (6) (2001) 705–707.
- [2] B. Korzh, et al., Demonstration of sub-3 ps temporal resolution with a superconducting nanowire single-photon detector, *Nature Photon.* 14 (4) (2020) 250–255.
- [3] F. Marsili, et al., Detecting single infrared photons with 93% system efficiency, *Nature Photon.* 7 (3) (2013) 210–214.
- [4] T. Polakovic, W. Armstrong, G. Karapetrov, Z.-E. Meziani, V. Novosad, Unconventional applications of superconducting nanowire single photon detectors, *Nanomaterials* 10 (6) (2020).
- [5] N. Sherman, Superconducting nuclear particle detector, *Physical Review Letters* 8 (11) (1962) 438.
- [6] N. Zen, Y. Chen, K. Suzuki, M. Ohkubo, S. Miki, Z. Wang, Development of superconducting strip line detectors (sslds) for time-of-flight mass spectrometers (tof-ms), *IEEE transactions on applied superconductivity* 19 (3) (2009) 354–357.
- [7] A. Casaburi, E. Esposito, M. Ejrnaes, K. Suzuki, M. Ohkubo, S. Pagano, R. Cristiano, A 2×2 mm² superconducting strip-line detector for high-performance time-of-flight mass spectrometry, *Superconductor Science and Technology* 25 (11) (2012) 115004.
- [8] M. Ohkubo, Superconducting detectors for particles from atoms to proteins, *Physica C: Superconductivity* 468 (15–20) (2008) 1987–1991.
- [9] K. Suzuki, S. Miki, S. Shiki, Y. Kobayashi, K. Chiba, Z. Wang, M. Ohkubo, Ultrafast ion detection by superconducting nbn thin-film nanowire detectors for time-of-flight mass spectrometry, *Physica C: Superconductivity* 468 (15–20) (2008) 2001–2003.
- [10] K. Sano, Y. Takahashi, Y. Yamanashi, N. Yoshikawa, N. Zen, M. Ohkubo, Demonstration of single-flux-quantum readout circuits for time-of-flight mass spectrometry systems using superconducting strip ion detectors, *Superconductor Science and Technology* 28 (7) (2015) 074003.
- [11] K. Suzuki, S. Shiki, M. Ukibe, M. Koike, S. Miki, Z. Wang, M. Ohkubo, Hot-spot detection model in superconducting nano-stripline detector for kev ions, *Applied physics express* 4 (8) (2011) 083101.
- [12] M. Strauß, et al., Highly sensitive single-molecule detection of macromolecule ion beams, *Science Advances* 9 (48) (2023) eadj2801.
- [13] H. Azzouz, S. N. Dorenbos, D. De Vries, E. B. Ureña, V. Zwiller, Efficient single particle detection with a superconducting nanowire, *AIP Advances* 2 (3) (2012) 032124.

[14] S. Lee, T. Polakovic, W. Armstrong, A. Dibos, T. Draher, N. Pastika, Z.-E. Meziani, V. Novosad, Beam tests of SNSPDs with 120 GeV protons, *Nucl. Instrum. Meth. A* 1069 (2024) 169956.

[15] C. Peña, et al., High energy particle detection with large area superconducting microwire array, *JINST* 20 (03) (2025) P03001.

[16] J. Ekin, *Experimental Techniques for Low-Temperature Measurements: Cryostat Design, Material Properties and Superconductor Critical-Current Testing*, Oxford University Press, 2006.

[17] M. J. Eshraghi, M. Cho, J. M. Kim, I. Sasada, Conducted emi reduction on the pulse tube cryocooler, *IEEE Transactions on Magnetics* 45 (6) (2009) 2754–2757.

[18] T. Polakovic, S. Lendinez, J. E. Pearson, A. Hoffmann, V. Yefremenko, C. L. Chang, W. Armstrong, K. Hafidi, G. Karapetrov, V. Novosad, Room temperature deposition of superconducting niobium nitride films by ion beam assisted sputtering, *APL Materials* 6 (7) (2018) 076107.

[19] M. Martin, Evaluated Nuclear Structure Data File - National Nuclear Data Center, *Nucl. Data Sheets* 114 (2013) 1497.

[20] J. H. Hubbell, S. M. Seltzer, Tables of x-ray mass attenuation coefficients and mass energy-absorption coefficients from 1 kev to 20 mev for elements z =1 to 92 and 48 additional substances of dosimetric interest, *Tech. Rep. NISTIR 5632*, National Institute of Standards and Technology, Gaithersburg, MD (2013).

[21] S. Guo, J. Tan, H. Zhang, J. Wang, T. Ji, L. Zhang, X. Hu, J. Chen, J. Xie, K. Zou, Y. Meng, X. Bei, L.-A. Wu, Q. Chen, H. Wang, X. Tu, X. Jia, Q.-Y. Zhao, L. Kang, P. Wu, High-timing-precision detection of single X-ray photons by superconducting nanowires, *National Science Review* 11 (1) (2023) nwad102.

[22] K. Inderbitzin, A. Engel, A. Schilling, K. Il'in, M. Siegel, An ultra-fast superconducting Nb nanowire single-photon detector for soft x-rays, *Applied Physics Letters* 101 (16) (2012) 162601.

[23] P. Gregshammer, H. W. Weber, R. T. Kampwirth, K. E. Gray, The effects of high-fluence neutron irradiation on the superconducting properties of magnetron sputtered NbN films, *Journal of Applied Physics* 64 (3) (1988) 1301–1306.

[24] A. B. Smith, P. T. Guenther, J. F. Whalen, Neutron total and scattering cross sections of niobium in the continuum region, *Zeitschrift für Physik* 264 (5) (1973) 379–398.

[25] S. P. Chockalingam, M. Chand, A. Kamlapure, J. Jesudasan, A. Mishra, V. Tripathi, P. Raychaudhuri, Tunneling studies in a homogeneously disordered *s*-wave superconductor: Nbn, *Phys. Rev. B* 79 (2009) 094509.

[26] E. Piatti, A. Sola, D. Daghero, G. A. Ummarino, F. Laviano, J. R. Nair, C. Gerbaldi, R. Cristiano, A. Casaburi, R. S. Gonnelli, Superconducting transition temperature modulation in nbn via edl gating, *Journal of Superconductivity and Novel Magnetism* 29 (3) (2016) 587–591.

[27] W. Zhang, Q. Jia, L. You, X. Ou, H. Huang, L. Zhang, H. Li, Z. Wang, X. Xie, Saturating intrinsic detection efficiency of superconducting nanowire single-photon detectors via defect engineering, *Phys. Rev. Appl.* 12 (2019) 044040.

[28] S. Strohauer, F. Wietschorke, L. Zugliani, R. Flaschmann, C. Schmid, S. Grotowski, M. Müller, B. Jonas, M. Althammer, R. Gross, K. Müller, J. J. Finley, Site-selective enhancement of superconducting nanowire single-photon detectors via local helium ion irradiation, *Advanced Quantum Technologies* 6 (12) (2023) 2300139.

[29] E. Batson, F. Incalza, M. Castellani, M. Colangelo, I. Charaev, A. Schilling, S. Cherednichenko, K. K. Berggren, Effects of helium ion exposure on the single-photon sensitivity of mgb₂ and nbn detectors, *IEEE Transactions on Applied Superconductivity* 34 (7) (2024) 1–6.